Int. J. Therm. Sci. (2000) 39, 498–504

S1290-0729(00)00205-2/FLA

Effect of interfacial phenomena on evaporative heat transfer in micro heat pipes [1]

Valérie Sartre, Mohamed Chaker Zaghdoudi, Monique Lallemand *

Centre de Thermique de Lyon, UPRESA CNRS 5008, INSA, 20 Av. Albert Einstein, 69621 Villeurbanne, France

(Received 15 September 1999, accepted 15 October 1999)

Abstract — A three-dimensional steady-state model for predicting heat transfer in a micro heat pipe array is presented. Three coupled models, solving the microregion equations, the two-dimensional wall heat conduction problem and the longitudinal capillary two-phase flow have been developed. The results, presented for an aluminium/ammonia triangular micro heat pipe array, show that the major part of the total heat input in the evaporator section goes through the microregion. In addition, both the apparent contact angle and the heat transfer rate in the microregion increase with an increasing wall superheat. It is also shown that the inner wall heat flux and temperatures as well as the contact angle decrease all along the evaporator section. © 2000 Éditions scientifiques et médicales Elsevier SAS

micro heat pipe / microregion / numerical simulation / heat transfer / contact angle

Résumé — **Influence des phénomènes interfaciaux sur les transferts de chaleur par évaporation dans les microcaloducs.** Un modèle tridimensionnel a été développé en régime permanent pour prédire les transferts thermiques au sein d'un microcaloduc. Ce modèle, composé de trois sous-modèles couplés, permet de résoudre les équations qui régissent les transferts dans la microrégion, le problème bidimensionnel de conduction thermique dans la paroi et l'écoulement capillaire axial liquide–vapeur. Les résultats, présentés pour une rangée de microcaloducs triangulaires aluminium/ammoniac, montrent qu'une grande partie du flux thermique imposé à l'évaporateur est évacuée par la microrégion. De plus, l'angle de contact apparent et la puissance thermique dissipée dans la microrégion augmentent avec la surchauffe de la paroi. On montre également que la densité de flux, la température de la paroi interne ainsi que l'angle de contact décroissent le long de l'évaporateur. © 2000 Éditions scientifiques et médicales Elsevier SAS

microcaloduc / microrégion / simulation numérique / transfert thermique / angle de contact

Nomenclature

A	cross-sectional area	m^2
A	Hamaker constant	J
d	width	m
g	gravity acceleration	$m{\cdot}s^{-2}$
h	heat transfer coefficient	$W{\cdot}m^{-2}{\cdot}K^{-1}$
Δh_v	latent heat of vaporisation	$J{\cdot}kg^{-1}$
l	length	m
MHP	micro heat pipe	
P	pressure	$N{\cdot}m^{-2}$
P^*	dimensionless pressure	
q	heat flux	$W{\cdot}m^{-2}$
q^*	dimensionless heat flux	
Q	heat transfer rate per unit length of MHP	$W{\cdot}m^{-1}$
r	radius of curvature	m
R	thermal resistance	$K{\cdot}m^2{\cdot}W^{-1}$
$\Re$	gas constant	$J{\cdot}kg^{-1}{\cdot}K^{-1}$
T	temperature	K
u, v	axial, radial velocity	$m{\cdot}s^{-1}$
z	axial coordinate	m

Greek symbols

α	contact angle	deg
δ	film thickness	m
δ^*	dimensionless film thickness	
η, ξ	coordinates	m
θ	tilt angle	deg
λ	thermal conductivity	$W{\cdot}m^{-1}{\cdot}K^{-1}$
μ	dynamic viscosity	$kg{\cdot}m^{-1}{\cdot}s^{-1}$
ρ	density	$kg{\cdot}m^{-3}$
σ	surface tension	$N{\cdot}m^{-1}$
τ	viscous shear	$N{\cdot}m^{-2}$

* Correspondence and reprints.
m.lal@cethil.insa-lyon.fr

[1] Based on a paper presented as a plenary talk at Eurotherm Seminar No. 57 "Microscale Heat Transfer", Poitiers, France, July 8–10, 1998.

Subscripts

a	apparent
ad	adiabatic section
c	condenser, capillary
e	evaporator, evaporation
i	interfacial
l	liquid
mic	microregion
max	maximum
sat	saturation
t	total
v	vapour
w	wall

1. INTRODUCTION

Micro heat pipes (MHP) are commonly used to act as efficient heat spreaders to eliminate hot spots and to reduce temperature gradients of electronic equipment [1]. A single MHP consists of a small noncircular channel that uses the sharp angled corner regions as liquid arteries. Several authors have studied the behaviour of MHP by a pressure balance between the shear stress and the capillary forces in the entire MHP [2–4]. As a result, several relevant parameters for the determination of the MHP heat transport capability have been identified. The most significant parameters are the contact angle and the amount of working fluid. To better determine the maximum acceptable wall temperature for a boundary condition of the second kind, the 3D heat transfer problem in the whole MHP has to be solved.

Many investigations have been conducted to predict heat transfer during evaporation from the extended meniscus. Some authors considered the simplified assumption of an interface temperature T_{iv} equal to the saturation temperature and a constant curvature of the interface. Wayner et al. [5] have shown that this assumption is not valid and they have introduced a microscopic interfacial concept. Indeed, the microscopic fluid flow and heat transfer control the macroscopic performance. So, in these models, when the liquid–vapour interface contacts the heated wall, the extended meniscus is typically divided into three regions: a macroscopic region, with a meniscus of constant mean curvature which is dominated by the capillary forces (intrinsic meniscus region), a transition region or microregion (evaporating thin film region) and a microscopic region which consists of an adsorbed film (non-evaporating region) where the disjoining forces predominate.

In several investigations [6–9] for small capillary grooves, the 2D energy equations have been solved in the wall and/or the liquid film for a given groove cross-section. So, the temperature and heat transfer coefficient have been assumed constant along the axial groove direction. Holm and Goplen [7] developed a model that combines the Wayner's model with a 1D analysis of the heat conduction for a trapezoidal groove. In that case, the microregion accounts for approximately 80 % of the heat dissipation from the wall. In heat pipes with open grooves, Stephan and Büsse [8] solved the 2D heat conduction problem. They have shown that about 45 % of the total heat goes through the microregion, value much lower than 94 % corresponding to the assumption of an interface temperature set constant, equal to the saturation temperature. More recently, Khrustalev and Faghri [10] solved the 2D momentum and energy equations for the liquid and the vapour so as to study the fluid flow effect on the heat transfer between the heated wall and the fluid, in a cross-section of a capillary groove.

Ma and Peterson [11] proposed a model for predicting the heat transfer coefficient and temperature variations along the axial direction of a grooved plate, which handles the effects of the capillary-induced flow in grooves. The results indicate that the heat transfer coefficient decreases and the wall temperature increases along the axial direction of the groove. In addition, the apparent contact angle variation along the flow direction is given.

The present study was undertaken in order to analyse the effect of the interfacial evaporation phenomena in the microregion on the thermal performance of a MHP. For that purpose, a model has been developed which combines Stephan's treatment in the microregion with a 2D solution of the wall heat conduction problem in a MHP cross-section. The fluid flow along the MHP is considered by using a previous pressure balance model [4] including the longitudinal variations of the contact angle.

2. THEORETICAL MODEL

For thermal control of electronic equipment, MHP arrays are often used [1]. The studied MHP array consists of an aluminium plate, 120 mm long, in which 19 parallel triangular tubes are machined. The cross-sectional geometry of each groove (*figure 1*) is an equilateral triangle, of width 0.7 mm, with an interchannel spacing of 0.2 mm. Ammonia is used as the working fluid at a saturation temperature of 27 °C. A uniform heat flux ($7.5 \cdot 10^4$ W·m^{-2}) is applied on the upper surface of the evaporator plate

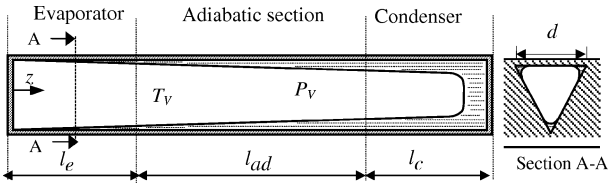

Figure 1. Schematic of a tube of the MHP array.

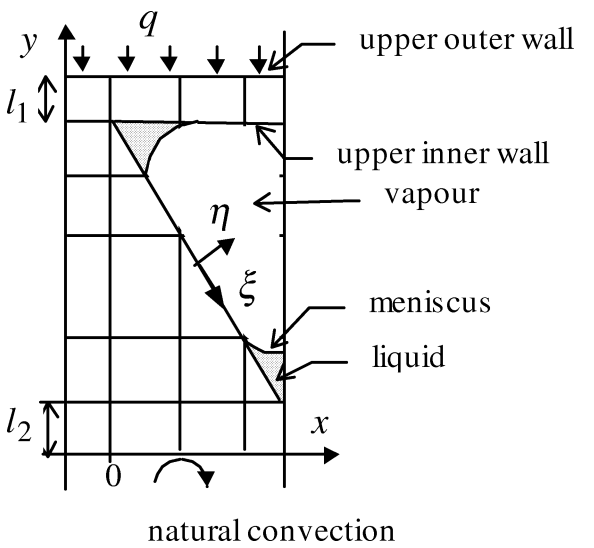

Figure 2. Cross section of the MHP plate.

TABLE I
Geometrical data (in mm).

d	l_1	l_2	l_e	l_c
0.7	0.1	0.1	10	5

and its lower surface is cooled by natural convection (*figure 2*). The condenser is water-cooled. The main geometrical MHP data are given in *table I*. In order to determine the thermal performance of such a system, the theoretical analysis of heat transfer can be done for a single tube.

2.1. Heat transfer in the microregion

The microregion model is based on the model developed by Stephan and Büsse [8]. In the evaporating thin film region (*figure 3*), the high evaporation rates induce a transverse liquid flow in the groove that is governed by two mechanisms: the surface tension forces and the adhesion forces. Moreover, the pressure drop along the flow generates a variation of the meniscus curvature radius in

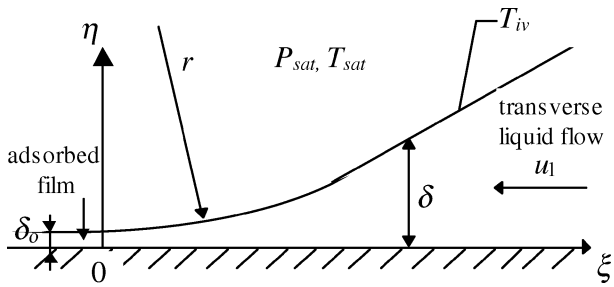

Figure 3. Schematic of the extended meniscus.

the flow direction. The second mechanism predominates when the meniscus is very close to the wall. For non-polar liquids as ammonia, the capillary pressure is given by

$$P_c = \frac{\sigma}{r} + \frac{A}{\delta^3} \tag{1}$$

The Hamaker constant A is equal to $2{\cdot}10^{-21}$ J for NH_3 [8]. Both the adhesion and surface tension forces reduce the liquid evaporation and cause an interfacial temperature increase. Thus, the equilibrium interface temperature T_{iv} is higher than the saturation temperature T_{sat}. T_{iv} is calculated by using the Clausius–Clapeyron equation:

$$T_{iv} = T_{sat}\left(1 + \frac{P_c}{\Delta h_v \rho_l}\right) \tag{2}$$

Assuming one-dimensional heat conduction through the liquid, normal to the wall, the heat flux transferred by the microregion can be written as [8]

$$q = (T_w - T_{iv})\left(\frac{\delta}{\lambda_l} + R_i\right)^{-1} \tag{3}$$

The wall temperature T_w in the microregion depends on the ξ-coordinate, the liquid thermal conductivity λ_l, and the interfacial resistance R_i, given by

$$R_i = \frac{T_{sat}\sqrt{2\pi \Re T_{sat}}}{\Delta h_v^2 \rho_v}\,\frac{(2-a)}{2a} \tag{4}$$

The accommodation coefficient a is equal to unity for an intensive evaporation [9].

The evaporating mass flux is deduced from the mass and momentum equations for the transverse liquid flow:

$$\dot{m}_e = -\frac{1}{3\mu_l}\frac{d}{d\xi}\left(\delta^3 \frac{dP_c}{d\xi}\right) \tag{5}$$

Combining (1), (3) and (5) leads to the following set of differential equations for determining the heat and mass transfer in the microregion as well as the meniscus shape:

$$\begin{aligned}
\frac{\mathrm{d}\delta}{\mathrm{d}\xi} &= \delta' \\
\frac{\mathrm{d}\delta'}{\mathrm{d}\xi} &= \frac{[1+\delta'^2]^{1.5}}{\sigma}\left(P_\mathrm{c} - \frac{A}{\delta^3}\right) \\
\frac{\mathrm{d}P_\mathrm{c}}{\mathrm{d}\xi} &= -\frac{3\mu_\mathrm{l} Q}{\Delta h_\mathrm{v}\rho_\mathrm{l}\delta^3} \\
\frac{\mathrm{d}Q}{\mathrm{d}\xi} &= \left(T_\mathrm{w} - T_\mathrm{sat}\left(1 + \frac{P_\mathrm{c}}{\Delta h_\mathrm{v}\rho_\mathrm{l}}\right)\right)\left(\frac{\delta}{\lambda_\mathrm{l}} + R_\mathrm{i}\right)^{-1}
\end{aligned} \tag{6}$$

The relevant boundary conditions at $\xi = 0$ are as follows:

$$\delta = \delta_0, \qquad \frac{1}{r} = 0, \qquad \frac{\mathrm{d}\delta}{\mathrm{d}\xi} = 0$$

2.2. Heat transfer in the MHP wall

The wall temperature is obtained by solving the 2D heat conduction problem inside the wall:

$$\nabla\big(\lambda_\mathrm{w}\nabla(T)\big) = 0 \tag{7}$$

Due to the symmetries of the MHP array, the studied region consists of a half tube and a half interchannel spacing. A uniform heat flux condition is imposed at the upper surface of the plate and a Fourier boundary condition at the lower surface (*figure 2*). The inner wall of the tube is divided into a dried part in contact with the vapour and a wetted part in contact with the liquid. In the dry part, the wall–vapour heat transfer is neglected. In the macroregion, heat is transferred by conduction from the wall to the liquid–vapour interface.

2.3. Capillary flow along the MHP

The capillary flow model is based on the steady-state 1D model developed by Longtin et al. [3]. In addition, the condenser section has been included in this model [4]. The MHP is divided into several control volumes for which the continuity, momentum and energy equations are written for the liquid and vapour phases and the Laplace–Young equation for the curvature radius of the liquid–vapour interface:

$$\frac{\mathrm{d}(A_\mathrm{v} u_\mathrm{v})}{\mathrm{d}z} = -A_\mathrm{i}\frac{\rho_\mathrm{l}}{\rho_\mathrm{v}}\,v_\mathrm{il} \tag{8}$$

$$\frac{\mathrm{d}(A_\mathrm{l} u_\mathrm{l})}{\mathrm{d}z} = A_\mathrm{i} v_\mathrm{il} \tag{9}$$

$$\rho_\mathrm{v}\frac{\mathrm{d}(A_\mathrm{l}u_\mathrm{l}^2)}{\mathrm{d}z}\,\mathrm{d}z = -\frac{\mathrm{d}(A_\mathrm{l}P_\mathrm{l})}{\mathrm{d}z}\,\mathrm{d}z - |\tau_\mathrm{il}|A_\mathrm{i} - |\tau_\mathrm{lw}|A_\mathrm{lw} - \rho_\mathrm{l}A_\mathrm{l}g\sin\theta\,\mathrm{d}z \tag{10}$$

$$\rho_\mathrm{v}\frac{\mathrm{d}(A_\mathrm{v}u_\mathrm{v}^2)}{\mathrm{d}z}\,\mathrm{d}z = -\frac{\mathrm{d}(A_\mathrm{v}P_\mathrm{v})}{\mathrm{d}z}\,\mathrm{d}z - |\tau_\mathrm{iv}|A_\mathrm{i} - |\tau_\mathrm{vw}|A_\mathrm{vw} - \rho_\mathrm{v}A_\mathrm{v}g\sin\theta\,\mathrm{d}z \tag{11}$$

$$v_\mathrm{il} = -\frac{Q_\mathrm{e}}{l_\mathrm{e}\rho_\mathrm{l}A_\mathrm{i}\Delta h_\mathrm{v}} \tag{12}$$

$$\frac{\mathrm{d}P_\mathrm{l}}{\mathrm{d}z} = \frac{\mathrm{d}P_\mathrm{v}}{\mathrm{d}z} - \frac{\mathrm{d}}{\mathrm{d}z}\left(\frac{\sigma}{r}\right) \tag{13}$$

The cross-sectional areas of the liquid, A_l, and the vapour, A_v, the liquid–vapour interfacial area, A_i, and the liquid–wall, A_l, and vapour–wall, A_v, contact surface areas are expressed as functions of the contact angle of the meniscus α and of the interfacial curvature radius. The resulting set of first-order, nonlinear, coupled ordinary differential equations is solved numerically to yield the five unknown variables: r, u_l, u_v, P_l and P_v, with the following boundary conditions:

$$\begin{aligned}
u_\mathrm{l}|_{z=0} &= u_\mathrm{v}|_{z=0} = 0 \\
u_\mathrm{l}|_{z=l_\mathrm{t}} &= u_\mathrm{v}|_{z=l_\mathrm{t}} = 0 \\
P_\mathrm{v}|_{z=0} &= P_\mathrm{sat} \\
P_\mathrm{l}|_{z=0} &= P_\mathrm{sat} - \frac{\sigma}{r|_{z=0}}
\end{aligned}$$

In the thermal model of the condenser section, three regions are considered in each MHP cross section. The first region is covered by a thin liquid film of constant thickness calculated by the Nüsselt theory. In the second region, the interfacial curvature varies linearly with the curvilinear interface abscissa. In the third region, the film curvature is constant. In the MHP model, an iterative procedure allows determination of the maximum heat transfer rate Q_max, assumed to be reached when the curvature radius of the meniscus is minimum at $z = 0$ and maximum at $z = l_\mathrm{t}$. The first case corresponds to $P_\mathrm{l} = 0$; r_max is achieved when the menisci just meet together.

3. NUMERICAL TREATMENT

The determination of heat transfer in the microregion, in the macroregion and in the wall and the capillary flow along the MHP requires different numerical approaches. Since all these equations are coupled together, they are solved by a numerical iterative method.

The set of the four differential equations (6) is solved numerically by the fourth-order Runge–Kutta integration

scheme. For given temperatures T_{sat} and T_w, the capillary pressure P_c at $\xi = 0$ is obtained from equation (2) ($T_{iv} = T_w$). The value of δ at $\xi = 0$ is calculated from equation (1) and the interface curvature is set to a very small value. The integration ends for the value of ξ where the capillary pressure effect on T_{iv} and the curvature change with ξ become negligible. The output of the microregion calculations are: the heat transfer coefficient h, δ (ξ), T_{iv} and the apparent contact angle $\alpha_a = \arctan(d\delta/d\xi)$.

For the 2D heat conduction through the wall, the studied region is divided into 19 regions, as shown in *figure 2*, for which the grid size is fixed. Thus, a grid refinement in the menisci area is allowed in this model. Equation (7) is solved numerically by an explicit finite difference method. The local heat transfer coefficients between the wall and the liquid are deduced from the microregion study and the local liquid film thickness determined by the capillary flow along the MHP. Computations are repeated until convergence between the input heat transfer rate and the heat transfer rate dissipated through the menisci and the bottom surface of the plate. The output of the 2D heat conduction problem is the wall temperature.

For the capillary flow, equations (8)–(13) and their boundary conditions are solved numerically. The numerical integration method is the fourth-order Runge–Kutta method. For a given contact angle, the MHP maximum heat transport is obtained.

For the whole MHP, the solving procedure for the heat transfer coefficient and the temperature distribution along the flow direction consists of the following steps:

(i) Solve the capillary flow equations along the MHP using a constant contact angle to determine the curvature radius of the meniscus distribution along the evaporator. For each evaporator cross section, the heat transfer coefficient distribution, deduced from the film thickness, is obtained.

(ii) Solve the microregion model with an initial wall temperature to find the heat transfer coefficient and the interfacial temperature profiles, which are input parameters of the wall conduction problem.

(iii) With the wall conduction model, update the temperature distribution of the wall for the three microregions.

(iv) Repeat steps (ii) and (iii) until convergence on the wall temperatures.

(v) Repeat steps (ii)–(iv) for several cross sections to obtain a contact angle distribution along the MHP. The whole procedure is repeated using the new contact angle distribution until a converged solution is obtained.

4. RESULTS AND DISCUSSION

Calculations were carried out for a MHP transporting heat between the evaporator (0.677 W per MHP) and a heat sink at a near constant temperature. Thus, the saturation temperature is approximately equal to 27 °C. *Figure 4* illustrates the dimensionless film thickness $\delta^* = \delta/\delta_{max}$, the dimensionless heat flux $q^* = q/q_{max}$ and the dimensionless capillary pressure $P_c^* = P_c/P_{c\,max}$ variations for the microregion. δ_{max}, q_{max} and $P_{c\,max}$ are equal to $3.55{\cdot}10^{-7}$ m, $1.65{\cdot}10^{8}$ W·m^{-2} and $2.34{\cdot}10^{6}$ Pa, respectively. The heat flux is initially zero in the adsorbed film and then it increases sharply at the beginning of the thin film evaporating region. Both the capillary pressure and the heat flux decrease with increasing values of the film thickness. The curvature of the liquid film in the microregion depends on α_a. For a given superheat $T_w - T_{iv}$, α_a increases rapidly with ξ (*figure 5*) and its maximum value corresponds to the contact angle α. It is also shown that α_a increases as the wall temperature increases. α depends greatly on the superheat, as seen in *figure 6*. The total heat transferred in the microregion per unit length of the MHP evaporator Q_{mic} is obtained by integrating equation (3) along the microregion. We observe that Q_{mic} increases with the superheat (*figure 6*).

As the liquid flows along the MHP axial direction, the liquid film profile, the contact angle and, hence, the temperature distribution vary. The curvature radius of the meniscus varies from its lowest value at the begin-

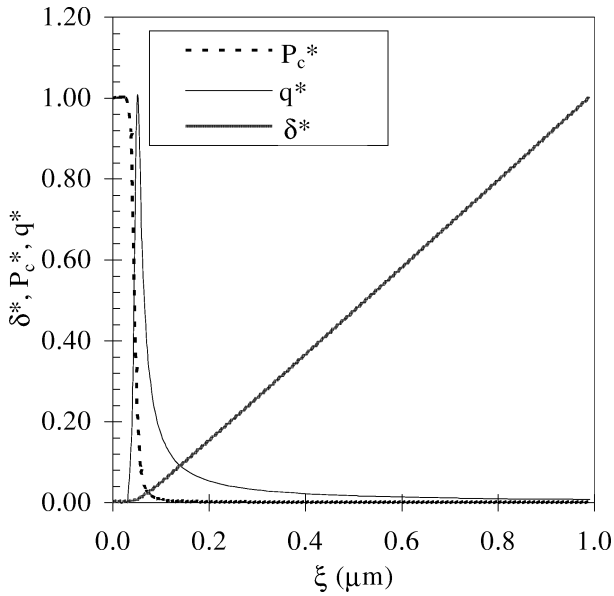

Figure 4. Heat flux, film thickness and capillary pressure in the microregion.

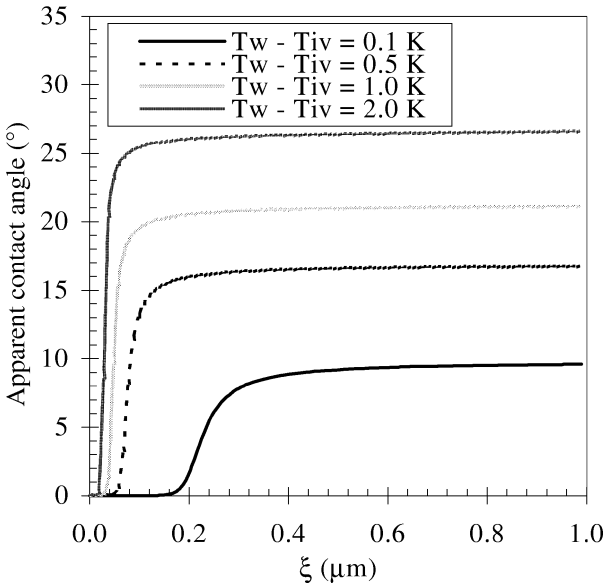

Figure 5. Superheat effect on the contact angle.

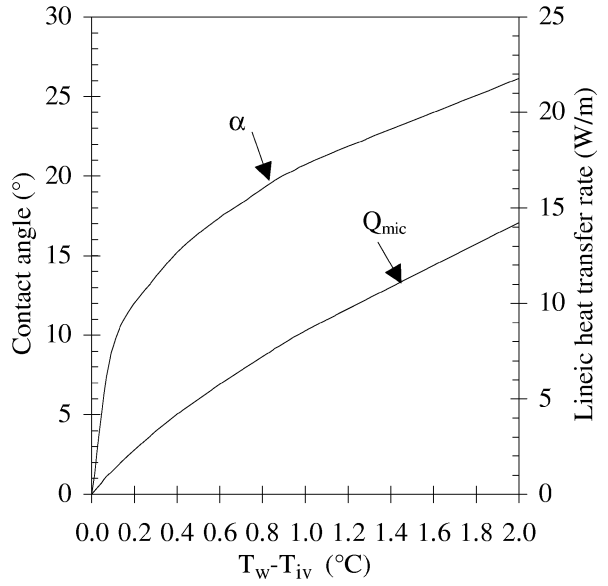

Figure 6. Superheat effect on the contact angle and linear heat transfer rate in the microregion.

ning of the evaporator ($z = 0$) to its highest value at the end ($z = l_e$) (*figure 7*). Therefore, the meniscus cross-sectional area increases too, which in turn increases the wetted wall width along the MHP evaporator (*figure 7*). *Figure 8* shows the heat flux along the upper inner wall, plotted from the corner of the MHP ($x = 0$), for two cross sections, $z = 0$ and $z = l_e$. At the end of the wetted region, beyond $x = 5$ μm and $x = 105$ μm for each section, respectively (*figure 7*), there is no heat flux through the dried region. For a given cross section, the heat flux increases from the corner to the end of the meniscus where it exhibits a sharp maximum in the microregion. The heat flux in the intrinsic meniscus is higher at $z = 0$ than that at $z = l_e$. This is due to the small heat transfer surface area at the beginning of the evaporator. Thus, as the linear heat transfer rate is uniform on the upper outer wall in the two sections, the upper inner wall heat flux, at $z = 0$, is higher. In addition, the heat transfer coefficients are higher at $z = 0$ than those at $z = l_e$ because the liquid film thickness is rather small. *Figure 9* shows

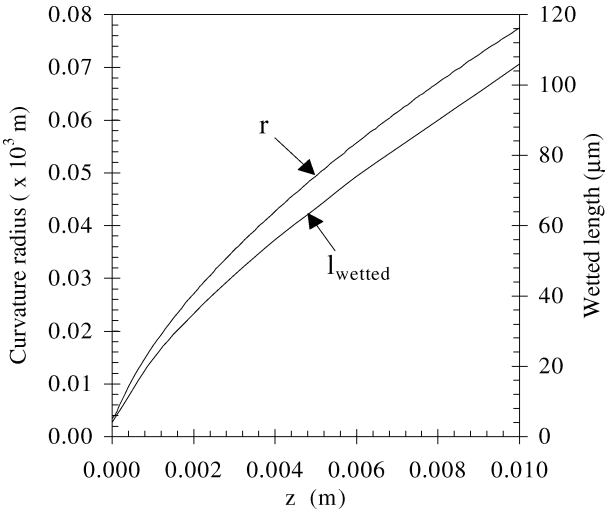

Figure 7. Curvature radius of the meniscus and wetted length distributions along the MHP evaporator.

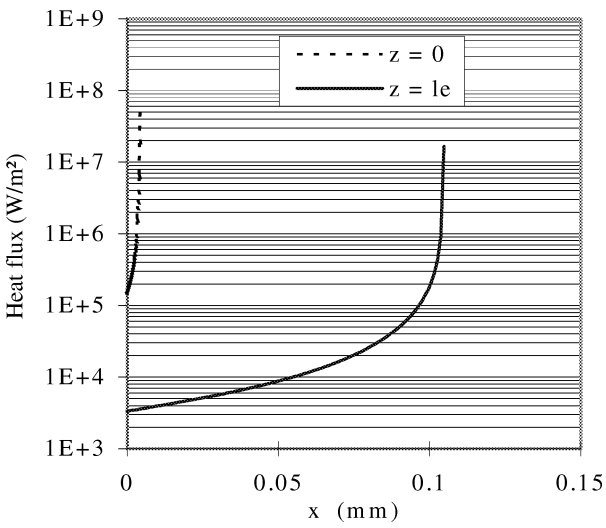

Figure 8. Heat flux distribution on the upper inner wall.

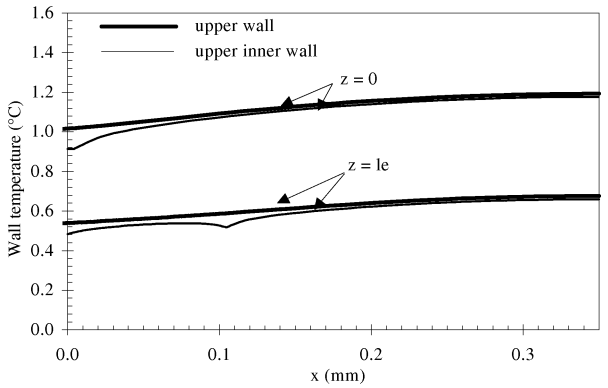

Figure 9. Temperature distribution on the upper inner and outer walls.

for each cross section the temperature profiles of the upper outer wall and of the upper inner wall, plotted from $x = 0$ to $x = d/2$ (MHP axis). For both cross sections, the wall temperatures increase from $x = 0$ to $x = d/2$. The maximum temperature is achieved at $x = d/2$, due to the weaker heat transfer between the dried wall and the vapour. The upper inner wall temperatures are minima in the microregion according to the very high heat flux dissipated in this area. The temperature levels are higher at the beginning than at the end of the evaporator because the heat transfer surface area between the wall and the liquid is small at $z = 0$. As a result of the superheat decrease along the MHP evaporator, the contact angle also decreases from $\alpha = 21°$ at $z = 0$ to $\alpha = 17°$ at $z = l_e$.

5. CONCLUSION

A theoretical model for predicting the heat transfer in a MHP array has been developed. This model considers the effect of the capillary flow along the MHP, the 2D heat conduction in the MHP wall and heat transfer in the micro- and macroregions. This model can be used to efficiently predict the contact angle, the wetted or dried area along the MHP, the wall temperatures, the heat flux distribution and the maximum heat transport capability. The most significant results indicate that:

(i) In the microregion, the apparent contact angle of the meniscus increases with an increasing wall superheat.

(ii) This apparent contact angle reaches a constant value when the disjoining pressure effects become negligible.

(iii) For our conditions, the wetted lengths are approximately 5 μm and 105 μm, at the beginning and at the end of the evaporator, respectively.

(iv) High heat transfer rates in the microregion are obtained, leading to the smallest superheats.

(v) The wall superheat and the contact angle decrease as the wall temperatures decrease along the MHP axial direction.

(vi) The local heat flux, as well as the local heat transfer coefficients, are both decreasing along the MHP axis.

Acknowledgements

This research has been carried out in the frame of the BRITE-EURAM Programme (KHIEPCOOL N° BE96-3028). In this project, the partners are industrial companies—Sextant Avionique, coordinator, Nokia and Electrovac—and universities—IKE and INSA. The authors gratefully acknowledge the financial support of the European Commission.

REFERENCES

[1] Groll M., Schneider M., Sartre V., Zaghdoudi M.C., Lallemand M., Thermal control of electronic equipment by heat pipes, Rev. Gén. Therm. 37 (5) (1998) 323–352.

[2] Babin B.R., Peterson G.P., Wu D., Steady-state modeling and testing of a micro heat pipe, J. Heat Tran. 112 (1990) 595–601.

[3] Longtin J.P., Badran B., Gerner F.M., A one dimensional model of a micro heat pipe during steady-state operation, J. Heat Tran. 116 (1994) 709–715.

[4] Zaghdoudi M.C., Sartre V., Lallemand M., Theoretical investigation of micro heat pipes performance, in: 10th International Heat Pipe Conference, Stuttgart, September 1997, p. 6.

[5] Wayner P.C., Kao Y.K., LaCroix L.V., The interline heat-transfer coefficient of an evaporating wetting film, Int. J. Heat Mass Tran. 19 (1976) 487–491.

[6] Kamotani Y., Evaporator film coefficients of grooved heat pipes, in: 3rd International Heat Pipe Conference, Palo Alto, California, 1978, pp. 128–130.

[7] Holm F.W., Goplen S.P., Heat transfer in the meniscus thin-film transition region, J. Heat Tran. 101 (1979) 543–547.

[8] Stephan P.C., Büsse C.A., Analysis of the heat transfer coefficient of grooved heat pipe evaporator walls, Int. J. Heat Mass Tran. 35 (2) (1992) 383–391.

[9] Khrustalev D., Faghri A., Heat transfer during evaporation on capillary-grooved structures of heat pipes, J. Heat Tran. 117 (1995) 740–747.

[10] Khrustalev D., Faghri A., Fluid flow effects in evaporation from liquid–vapor meniscus, J. Heat Tran. 118 (1996) 725–730.

[11] Ma H.B., Peterson G.P., Temperature variation and heat transfer in triangular grooves with an evaporating film, Journal of Thermophysics and Heat Transfer 11 (1) (1997) 90–97.